Geophysical Research Letters

RESEARCH LETTER
10.1029/2025GL115001

Global Observations of Acetyl Peroxynitrate (PAN) in the Remote Troposphere

Young Ro Lee[1], L. Gregory Huey[1], David J. Tanner[1], James M. Roberts[2], Yuhang Wang[1], Paul O. Wennberg[3], John D. Crounse[3], Hannah Allen[3], Eric C. Apel[4], Alan J. Hills[4], Rebecca S. Hornbrook[4], James W. Elkins[5], Eric Hintsa[5,6], Fred Moore[5,6], Samuel R. Hall[4], Kirk Ullmann[4], Kathryn McKain[5], Colm Sweeney[5], Thomas B. Ryerson[2], Jeff Peischl[2,6], Chelsea R. Tompson[2,6], Ilann Bourgeois[2,6], Eric Ray[2,6], Paul A. Newman[7], and Sarah Strode[7,8]

[1]School of Earth and Atmospheric Sciences, Georgia Institute of Technology, Atlanta, GA, USA, [2]NOAA Chemical Sciences Laboratory, Boulder, CO, USA, [3]Division of Geological and Planetary Sciences, California Institute of Technology, Pasadena, CA, USA, [4]Atmospheric Chemistry Observations & Modeling, NSF National Center for Atmospheric Research, Boulder, CO, USA, [5]NOAA Global Monitoring Laboratory, Boulder, CO, USA, [6]Cooperative Institute for Research in Environmental Sciences, University of Colorado, Boulder, CO, USA, [7]NASA Goddard Space Flight Center, Greenbelt, MD, USA, [8]Morgan State University, GESTAR-II, Baltimore, MD, USA

Abstract We present global airborne observations of acetyl peroxynitrate ($CH_3C(O)OONO_2$, PAN) in the remote troposphere from the Atmospheric Tomography (ATom) campaign. These observations show that biomass burning is the dominant source of PAN in the Southern Hemisphere (SH). In the Northern Hemisphere, anthropogenic emissions from Asia and Europe also contribute significantly to PAN over the Pacific and Atlantic Oceans. Model simulations underestimate PAN in the lower troposphere, in part, due to the underestimation of local production driven by acetaldehyde oxidation and β_{NO_2} (the ratio of acetyl peroxy radicals reacting with NO_2 relative to other pathways). The significant impacts of biomass burning evident in the ATom PAN observations suggest that improving model treatment of plume transport and the conversion of NO_x to PAN in biomass burning plumes is a viable focus for better simulating PAN. Global observations of PAN provide a benchmark for the evaluation of satellite observations and model simulations of PAN.

Plain Language Summary We report the global airborne observations of acetyl peroxynitrate (PAN) from the Atmospheric Tomography (ATom) campaign. Biomass burning is the dominant source of PAN over the remote oceans in the Southern Hemisphere. Anthropogenic emissions from Asia and Europe significantly contribute to PAN levels over the Pacific and Atlantic Oceans, alongside biomass burning. Model simulations underestimate PAN in the lower oceanic troposphere, partly due to an underestimation in local production driven by acetaldehyde. Our observations show strong evidence of the persistent biomass burning influence on PAN throughout the remote troposphere, particularly over the Southern Hemispheric oceans. This work provides a valuable data set to improve understanding of the global distribution of PAN.

Key Points:

- Global airborne observations of PAN over the remote troposphere during the ATom campaign are presented
- Biomass burning emissions are the dominant source of PAN over the Southern Hemispheric oceans, while in the Northern Hemisphere (NH), anthropogenic emissions from Asia and Europe significantly contribute to the remote tropospheric PAN levels alongside biomass burning
- Model simulations underestimate the local production of PAN in the lower oceanic troposphere, driven by acetaldehyde, as well as the impact of biomass burning on PAN levels throughout the remote troposphere

Supporting Information:

Supporting Information may be found in the online version of this article.

Correspondence to:

L. G. Huey,
greg.huey@eas.gatech.edu

Citation:

Lee, Y. R., Huey, L. G., Tanner, D. J., Roberts, J. M., Wang, Y., Wennberg, P. O., et al. (2025). Global observations of acetyl peroxynitrate (PAN) in the remote troposphere. *Geophysical Research Letters*, *52*, e2025GL115001. https://doi.org/10.1029/2025GL115001

Received 3 FEB 2025
Accepted 28 JUL 2025

Author Contributions:

Conceptualization: Young Ro Lee
Data curation: Young Ro Lee
Formal analysis: Young Ro Lee, James M. Roberts
Funding acquisition: L. Gregory Huey
Methodology: Young Ro Lee, David J. Tanner
Supervision: L. Gregory Huey
Writing – original draft: Young Ro Lee

1. Introduction

Acetyl peroxynitrate (PAN) is an important reservoir for nitrogen oxides (NO_x). In many regions of the troposphere, PAN is the primary form of reactive nitrogen (NO_y) (Roberts, 2007). PAN can undergo long-range transport as it is insoluble and quite stable at cold temperatures (lifetime of PAN, τ_{PAN}, up to a month in the upper troposphere) (Frenzel et al., 2000; Singh & Hanst, 1981; Talukdar et al., 1995). Transport and subsequent thermolysis of PAN to release NO_x is often essential for photochemical ozone (O_3) production in the remote troposphere, where NO_x is limited (Fischer et al., 2014; Kasibhatla et al., 1993; Moxim et al., 1996).

Despite significant advances in understanding the distribution of PAN on a global scale, large uncertainties persist in the remote troposphere. Previous studies attributed pollution episodes in remote marine environments, where PAN is a major component of NO_y, to continental transport from urban areas, biomass burning and lightning-NO_x emissions (e.g., Blake et al., 1999; Fischer et al., 2014; Roberts et al., 2004; Singh et al., 1996, 2006, 2009; Wahner et al., 1994). However, the global impact of these sources, particularly in remote regions like the Southern Hemisphere (SH) oceans, remains poorly characterized. Observations in these regions are scarce but are critical for diagnosing the key factors controlling the global distribution of PAN including changing impacts of

Writing – review & editing: Young Ro Lee, L. Gregory Huey, David J. Tanner, James M. Roberts, Yuhang Wang, Paul O. Wennberg, John D. Crounse, Hannah Allen, Eric C. Apel, Alan J. Hills, Rebecca S. Hornbrook, James W. Elkins, Eric Hintsa, Fred Moore, Samuel R. Hall, Kirk Ullmann, Kathryn McKain, Colm Sweeney, Thomas B. Ryerson, Jeff Peischl, Chelsea R. Tompson, Ilann Bourgeois, Eric Ray, Paul A. Newman

continental emissions, transport, and the atmospheric chemistry of pollutants transported to the remote troposphere (Roberts, 2007). Recent studies from the NASA Atmospheric Tomography (ATom) campaign, considered here, emphasize gaps in understanding remote tropospheric composition. These include missing sources of primary PAN precursors such as acetaldehyde and NO_x over remote oceans (Shah et al., 2023; S. Wang et al., 2019), and the significant contribution of biomass burning to the global distribution of O_3, peroxides and particles (Allen et al., 2022; Bourgeois et al., 2021; Schill et al., 2020). Observations of PAN in the remote troposphere, in combination with satellite observations and model simulations, are also critical for addressing gaps in our understanding (Zhai et al., 2024).

In this work, we present global-scale airborne PAN observations with high temporal resolution and extensive spatial coverage from the ATom campaign (Thompson et al., 2021). These observations provide "background" levels of PAN and its precursors in regions previously lacking extensive measurements, achieved through near-continuous vertical sampling and flight strategies designed for an unbiased assessment of the remote troposphere. We report PAN mixing ratios over the remote Pacific and Atlantic Oceans in all seasons. We examine remote tropospheric PAN using observations and model simulations including emission tracer measurements, back-trajectory analyses, and tagged emission tracer simulations. A diagnostic evaluation of both PAN and its precursor simulations from a Chemical Transport Model (CTM) was performed using observations and kinetic calculations highly constrained by measured parameters. Lastly, we utilize measurements of biomass burning tracers and simulated biomass burning contributions to carbon monoxide (CO) to investigate the impact of biomass burning on the relationship between observed and simulated PAN.

2. Methods

A comprehensive suite of chemical, physical and meteorological measurements was obtained aboard the NASA DC-8 research aircraft during the four ATom deployments from 28 July 2016 (ATom–1) to 21 May 2018 (ATom–4). Each deployment, lasting for approximately 1 month in each season, followed near-identical flight plans that systematically sampled altitudes from 0.15 to 13 km over remote oceans as described by Figure S1a in Supporting Information S1 and Thompson et al. (2021). Instrumentation details are provided in Table S1 in Supporting Information S1. Data were merged to either a 10-s time base or the Trace Organic Gas Analyzer (TOGA) sampling interval (35 s of integrated sampling every 2 min) and filtered to exclude data obtained over land. The geographical boundaries (60°S–55°N; 67°W–180°E and 0–67°W for the Pacific and Atlantic Oceans, respectively) used to identify the data over ocean are illustrated along with the flight tracks in Figure S1b in Supporting Information S1. We removed data with stratospheric influence defined as when O_3 and O_3/CO were greater than 100 and 1 ppbv ppbv^{-1}, respectively, at altitudes greater than 6 km. A marked decrease in CFC-113 provided an additional proxy for stratospheric influence, employing the 25th-percentile values ranging from 70 to 72 pptv across each deployment as a cut-off. This effectively excluded data obtained at the edges of stratospheric-influenced samples that often have O_3 mixing ratios lower than 100 ppbv (Figure S2 in Supporting Information S1). Data in which the photolysis rate of J_{NO_2} was below its tenth percentile were excluded in kinetic calculations.

The ATom data set includes model products and trajectory calculations. To investigate the potential impact of transpacific transport, 10-day back trajectory ensembles, initialized at each minute along the ATom flight tracks, were utilized (Ray, 2021). Data points whose back trajectories intersected the boundaries of East Asia (16–55°N, 78–146°E) were identified as having "East Asian influence (East Asian influence (EAI))" (Figure S1b in Supporting Information S1). As transpacific transport is a complex process unlikely to be fully represented using a single method, we assessed systematic differences in measured chemical tracers such as CO, hydrogen cyanide (HCN), propionyl peroxynitrate (PPN) and PAN, for data with and without EAI. This analysis is facilitated by the Goddard Earth Observing System Version 5 (GEOS-5) simulations of tagged-CO concentrations, which well predicted the distribution, source, and episodic enhancements of CO during ATom–1 (Newman & Pawson, 2021; Strode et al., 2018). Our method to identify EAI is illustrated in Text S2 and Figures S3 and S4 in Supporting Information S1 using data from the 6 October 2017 research flight, which captured transpacific transport and SH biomass burning events.

A key focus of ATom is to provide observations to evaluate model-simulated remote tropospheric composition, previously hindered by a lack of relevant observations in such regions. For this purpose, we utilized outputs from the Global Modeling Initiative (GMI)-CTM (Strode et al., 2021). The performance of different CTMs has been

discussed elsewhere (e.g., Shah et al., 2023; Travis et al., 2020). Briefly, the GMI-CTM provides trace gas mixing ratios with a spatial resolution of 1° latitude × 1.25° longitude × 72 vertical levels and a temporal resolution of 15 min, interpolated to the ATom flight tracks (Strode et al., 2021). The same criteria used to filter observations were applied to the model outputs. For a diagnostic analysis of modeled PAN, we compared the model outputs with the observed precursors of PAN, as well as the estimated acetyl peroxy (PA) radical concentrations. The impact of observation-model discrepancies in these variables on PAN simulations are investigated by comparing the simulated PAN to observations and steady state (SS) calculation for PAN when temperatures were above 290 K, the median value observed in the lower troposphere (<2 km) during ATom. This allows identification of data in which the SS estimation for PAN is most valid. In addition, SS analysis enables assessment of PAN and precursor compatibility using improved measurements (S. Wang et al., 2019), overcoming past limitations from acetaldehyde artifacts (Staudt et al., 2003). The details in the calculations and estimated uncertainties are described in Supporting Information S1.

3. Results

3.1. PAN Mixing Ratios

Figure 1a illustrates the vertical profiles of median PAN mixing ratios in 1-km altitude bins over the tropics (0°–20°), mid-latitudes (20°–60°), and polar regions (60°–90°) in the Northern Hemisphere (NH) and SH in each season. In the NH lower troposphere, PAN mixing ratios were generally greater in the extratropics than in the tropics. A notable exception was observed in July–August, where the highest PAN mixing ratios (median of 20 pptv) were measured in the tropical lower troposphere. This coincided with the highest seasonal median PAN production rate (P_{PAN}, 13 pptv hr^{-1}) and acetaldehyde (278 pptv), along with the shortest $\tau_{PAN} \sim 0.8$ hr, suggesting efficient local PAN production. The latitudinal differences in vertical PAN mixing ratios are particularly noticeable in April–May, when PAN in the extratropics was greater than that in the tropics at all altitudes. Springtime enhancements of PAN in the NH remote extratropics have been attributed to the transport of continental outflow when photochemical production of PAN is efficient and its thermal decomposition is relatively slow (Bottenheim et al., 1994; Penkett & Brice, 1986).

On average, PAN in the NH increased with altitude from the low to mid-troposphere but decreased above 8 km, partly due to reduced photochemical production and loss by photolysis in the upper troposphere. In the SH, PAN also leveled off in the upper troposphere. Increasing PAN mixing ratios with altitude were associated with increasing τ_{PAN} and concurrent enhancements of combustion tracers such as CO and HCN. The contribution of local P_{PAN}, dominated by acetaldehyde oxidation, to this vertical distribution was minimal (Figure S5 in Supporting Information S1). Net P_{PAN} (P_{PAN}-loss rate of PAN, L_{PAN}) were below 1pptv hr^{-1} in the free troposphere over both the Pacific and Atlantic Oceans. In July–August, high PAN mixing ratios persisted above 8 km in all latitude bins. The elevated PAN coincided with HCN up to 680 pptv and a high probability of convective influence (3.5 times the annual median in the upper troposphere), which was estimated based on the back trajectories and satellite cloud detection as used by Allen et al. (2022) to examine global peroxide distributions during ATom. This suggests that transport of biomass burning plumes coupled with convection is critical to explain the NH PAN distribution in summer.

Unlike the complicated latitudinal distribution of PAN in the NH, PAN in the SH increased almost linearly at roughly 0.7 pptv per degree latitude from the South Pole to the tropics on average. We attribute the latitudinal gradient of PAN in the SH to increasing biomass burning impacts from Africa, South America, and Australia over the SH tropics. Median PAN mixing ratios in the mid- and upper troposphere were significantly greater in austral winter (July–August) and spring (September–October), the dry seasons with frequent burning events (Andreae et al., 2012; Paton-Walsh et al., 2022). The highest median value of PAN was observed at 6–8 km during austral spring. This springtime PAN maximum in the SH agrees with previous studies including recent satellite observations (Fischer et al., 2014; Pope et al., 2016). Based on strong correlations of PAN with biomass burning tracers (Section 3.2), we attribute the austral spring PAN maximum as well as most of the SH PAN variations to biomass burning.

Figures 1b and 1c show median PAN mixing ratios and PAN/NO_y ratios in 4-degree latitude and 1-km altitude bins, respectively. Elevated levels of PAN and its contribution to NO_y were observed throughout the NH extratropical troposphere. PAN remained a major component of NO_y in both the NH and SH extratropical free troposphere but was depleted in the tropical lower troposphere, consistent with previous remote surface measurements of PAN

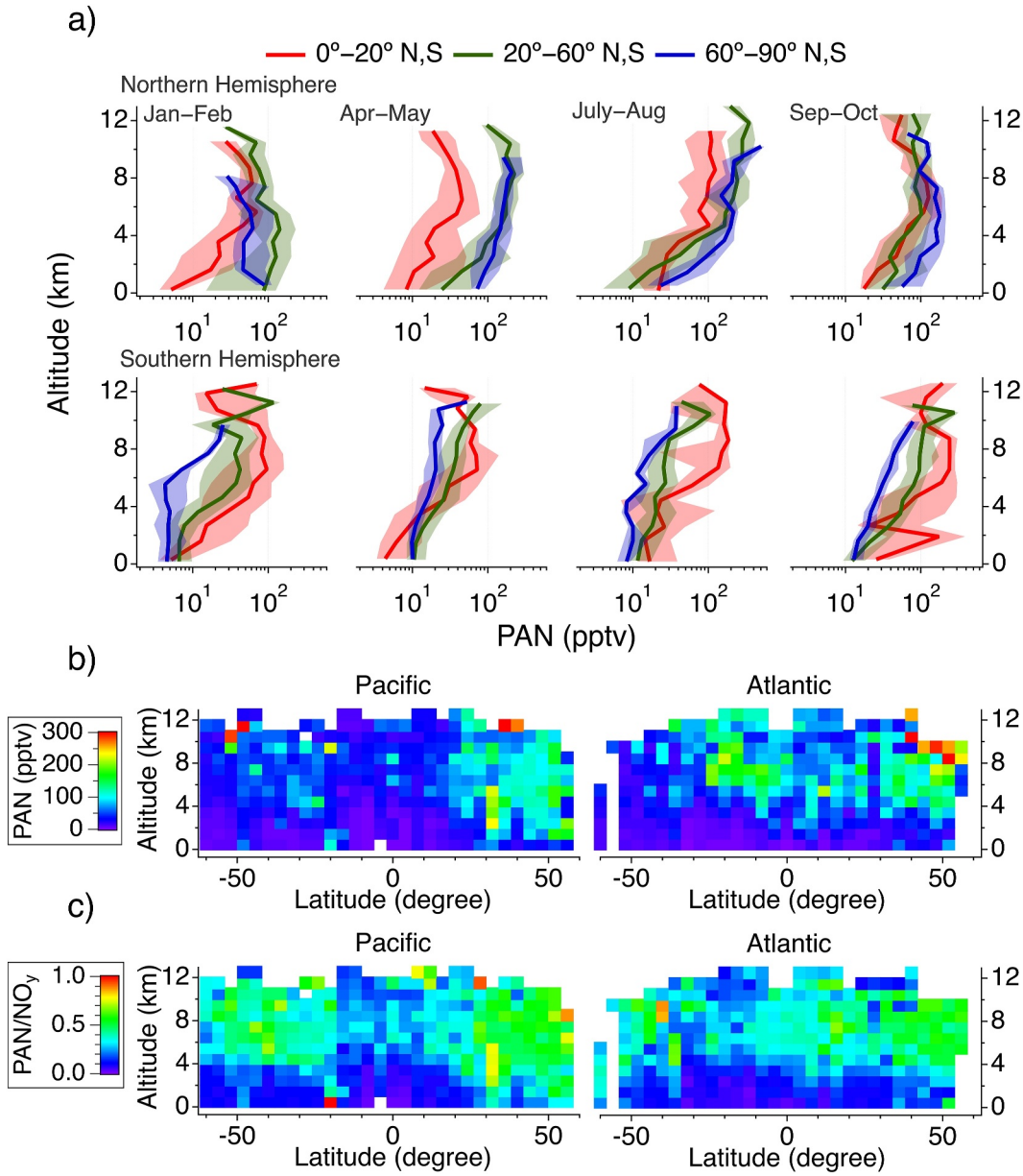

Figure 1. (a) Vertical profiles of median acetyl peroxynitrate (PAN) mixing ratios in 1-km altitude bins over the tropics (red), mid-latitudes (green), and polar regions (blue) of the Northern Hemisphere (top panels) and Southern Hemisphere (bottom panels), with shaded areas indicating 25th and 75th percentiles. Altitude plots of (b) PAN and (c) PAN to NO_y ratios as a function of latitude using data from all four ATom deployments.

(e.g., Rudolph et al., 1987; Müller & Rudolph, 1992; Roberts, 2007 and references therein). Our work attributes low PAN mixing ratios in the tropics to a net negative PAN production rate (median of P-L = −0.6 pptv hr^{-1}) driven by thermal decomposition combined with low NO_x levels over remote tropical oceans. Over the tropical Pacific Ocean, the patterns in latitude-altitude cross sections of PAN were consistent with those in L_{PAN} (Figure 1b and Figure S5d in Supporting Information S1). Despite the similarity of L_{PAN} over the Atlantic Ocean to the global trend, PAN was more than 30% of NO_y throughout the tropical Atlantic troposphere. This is consistent with strong enhancements of HCN (>200 pptv) and CO (>100 ppbv) throughout the subtropical Atlantic troposphere (Figures S6a and S6b in Supporting Information S1), indicating the influence of biomass burning on PAN and its contribution to NO_y in the regions. Consequently, PAN and PAN/NO_y over the Atlantic Ocean were more consistent

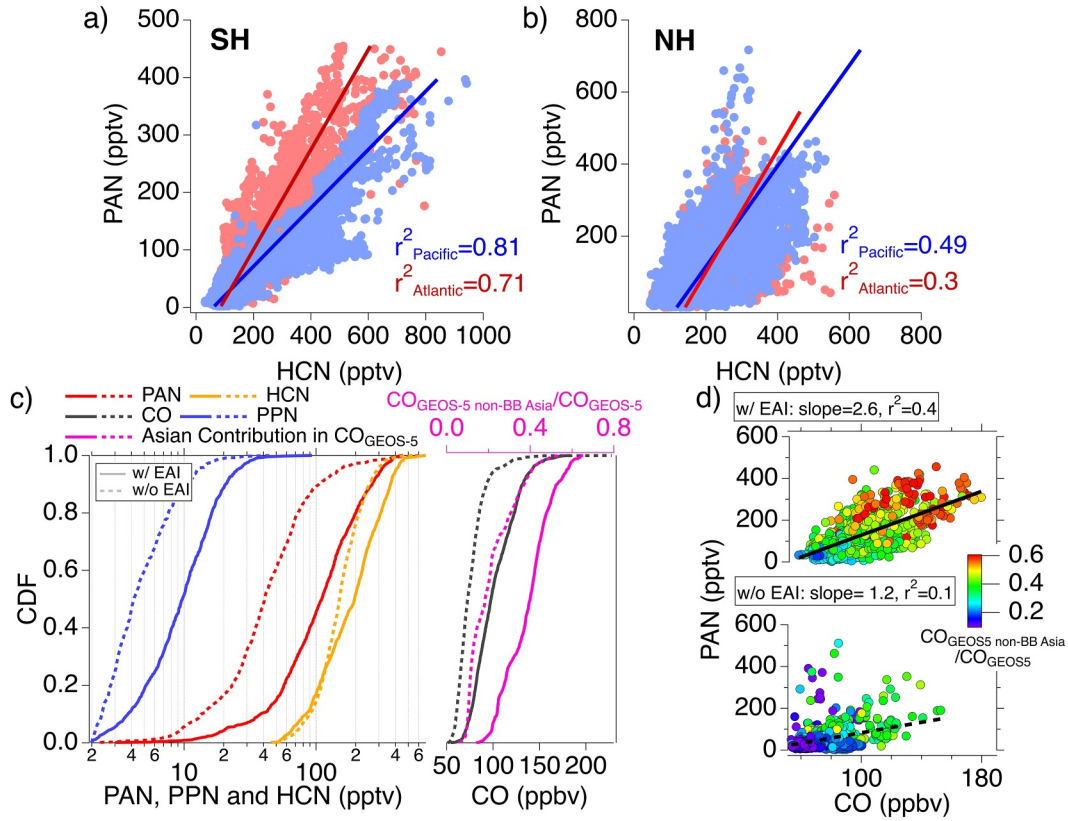

Figure 2. Scatter plot of observed acetyl peroxynitrate (PAN) versus hydrogen cyanide (HCN) for (a) the Southern Hemisphere oceans and (b) the Northern Hemisphere (NH) oceans. (c) Cumulative Distribution Functions of observed PAN, propionyl peroxynitrate, HCN, and CO and the fractional contributions of modeled CO from non-biomass burning Asian sources in GEOS-5 ($CO_{GEOS\text{-}5\ non\text{-}BB\ Asia}$) over the NH Pacific Ocean. Solid and dashed lines represent data with and without East Asian influence (EAI), respectively. (d) Scatter plots of observed PAN versus CO (top) with and (bottom) without EAI colored using $CO_{GEOS\text{-}5\ non\text{-}BB\ Asia}$ to the total CO ratios in GEOS-5.

across latitudes and altitudes in contrast to the significant variations observed between the NH and SH Pacific Oceans.

3.2. Sources of PAN

We investigate the influence of continental sources on PAN in the remote mid- and upper troposphere (altitudes >4 km), with τ_{PAN} up to 3 weeks, using chemical tracers of specific pollution sources and data categorized by back-trajectory analysis. Namely, we used high temporal resolution measurements of HCN and CO from biomass burning and general combustion emissions, respectively (Holzinger et al., 1999). PPN was used as a photochemical tracer of anthropogenic emissions, as it is formed almost exclusively from anthropogenic VOCs (Lee et al., 2021; Roberts, 2007; Toma et al., 2019). PPN measurements were not available for July–August (ATom-1).

Despite the wide geographic coverage of the data, a strong correlation ($r^2 > 0.7$) between PAN and HCN was notable over the SH Oceans (Figure 2a), highlighting the significant contribution of biomass burning to PAN in these regions. This chemical tracer analysis was further facilitated by TOGA measurements of two anthropogenic tracers, C_2Cl_4 and CH_2Cl_2, and a biomass burning tracer CH_3CN (Apel et al., 2015; Roozitalab et al., 2024). The analysis using TOGA measurements was consistent with results from the faster time response measurements. The correlations of PAN, CO, and PPN with the biomass burning tracers (HCN and CH_3CN) were significantly higher than those with the anthropogenic tracers measured by TOGA. Figures S7a and S7b in Supporting Information S1 illustrates the seasonal trends of PAN and chemical tracers using box plots. The marked increases in PAN during the SH fire seasons (September–October) were consistent with those of HCN and CO for both the SH Pacific and

Atlantic Oceans (Figures S7a and S7b in Supporting Information S1). For this reason, this work suggests that biomass burning is the primary contributor to PAN and pollutant distribution in the SH.

PAN showed moderate correlations with HCN over the NH Pacific and Atlantic Oceans (r^2 = 0.5 and 0.3, respectively), indicating a notable contribution of biomass burning transport to PAN in the NH (Figure 2b). Over the NH Pacific Ocean, the correlations of PAN and CO with C_2Cl_4 and CH_2Cl_2 were similar to those with HCN, suggesting that anthropogenic emissions are also important contributors to PAN over this region. Consistent with this, the seasonal trends of PAN were more comparable to those of HCN than those of CO for both the NH Pacific and Atlantic Oceans (Figures S7c and S7d in Supporting Information S1). PPN showed moderate correlations with anthropogenic (r^2 of 0.4 and 0.3 with C_2Cl_4 and CH_2Cl_2, respectively) and burning ($r^2 > 0.3$ with CH_3CN) tracers only over the NH Pacific Ocean and SH Oceans, respectively. While PAN and PPN showed a negligible relationship with anthropogenic tracers including CO over the NH Atlantic Ocean, increasing PAN mixing ratios were often coincident with elevations in the observed propane mixing ratios and the fractional contribution of CO from European non-biomass burning source ($CO_{non\text{-}BB\ EU}$) in GEOS-5 simulations in the extratropical regions (Figure S8 in Supporting Information S1). The highest PAN and propane reached up to 400 and 1.3 ppbv, respectively, along with greater than 60% combined contribution of $CO_{non\text{-}BB\ EU}$ and CO from Asian non-biomass burning sources ($CO_{non\text{-}BB\ Asia}$) in GEOS-5. Consequently, this suggests that enhancements of PAN in the NH Atlantic extratropical regions may be more associated with anthropogenic emissions from Europe and Asia than from North America.

The observed relationships between PAN and chemical tracers point out the important contribution of both anthropogenic and biomass burning emissions to PAN levels over the NH Pacific Ocean. An important anthropogenic pollution source in the NH Pacific Ocean is transpacific transport from East Asia (Roberts et al., 2004; Y. Wang et al., 2003), with its strongest influence in spring (J. Liu et al., 2005; Stohl et al., 2002). Figure 2c shows cumulative distribution functions (CDFs) of PAN and related tracers with and without EAI, determined from the back trajectories, using mid- and upper tropospheric data for the NH. Based on the CDFs in Figure 2c, data with EAI contained elevated levels of PAN and tracers, with mixing ratios of PAN, CO, HCN, and PPN being 2.7, 1.3, 1.3, and 2.3 times higher, respectively, compared to those without EAI. The elevated levels of CO are consistent with a 26% higher fractional contribution of $CO_{non\text{-}BB\ Asia}$ to the total CO in GEOS-5 simulations. Similar systematic differences in PAN levels have been reported by previous observations. For example, airborne measurements during ITCT 2K2 (Intercontinental Transport and Chemical Transformation 2002) campaign observed up to 650 pptv of PAN accompanied with CO mixing ratios above 150 ppbv (Nowak et al., 2004; Roberts et al., 2004). In accordance with these findings, Figure 2d illustrates data with EAI contain higher levels of both PAN and CO, along with larger slopes and r^2 for linear regressions between PAN and CO, as well as the higher fractional contribution of $CO_{non\text{-}BB\ Asia}$. Among data with EAI, median PAN mixing ratios peaked in spring with a value ~70% greater than the annual median. This seasonal trend agrees with the stronger impacts of transpacific transport on pollution over the Pacific Ocean during springtime (Jaffe et al., 1999; Zhang et al., 2008). Whereas biomass burning in East Asia is also active in spring, its role in EAI is likely minor, suggested by ~90% contribution of non-biomass burning CO in GEOS-5 simulations, consistent with recent satellite-based analysis of transpacific transport (Zhai et al., 2024).

3.3. Diagnostic Evaluation of Modeled PAN Using Observations

Figure 3a illustrates the probability distribution function of observed and modeled acetaldehyde and β_{NO_2}, where β_{NO_2} represents the ratio of PA reacting with NO_2 to the total reacting with NO, NO_2, HO_2, and RO_2. When PAN approaches SS due to rapid thermal decomposition over the remote lower troposphere, its concentration depends linearly on the production rate of PA, primarily driven by the oxidation of acetaldehyde by the OH radical (e.g., Figure S5 in Supporting Information S1), but inversely on the product of the thermal decomposition rate and $1/\beta_{NO_2} - 1$ (Sillman et al., 1990). On average, the model underestimated both acetaldehyde and β_{NO_2} when using steady-state NO_2 ($\beta_{SS\text{-}NO_2}$). In this section, NO_2 from pseudo-steady state (SS-NO_2) calculations is used due to potential measurement interferences from thermally labile species and a larger discrepancy between the observed NO_2 and the estimated values based on SS calculations and model simulations at higher altitudes (Nault et al., 2015; Shah et al., 2023). The persistent model underestimation of acetaldehyde across all altitudes supports findings from S. Wang et al. (2019) that attributed missing sources of acetaldehyde to oceanic emissions, aerosol photodegradation and unidentified sources during ATom 1–2. Measurement artifacts that may have previously

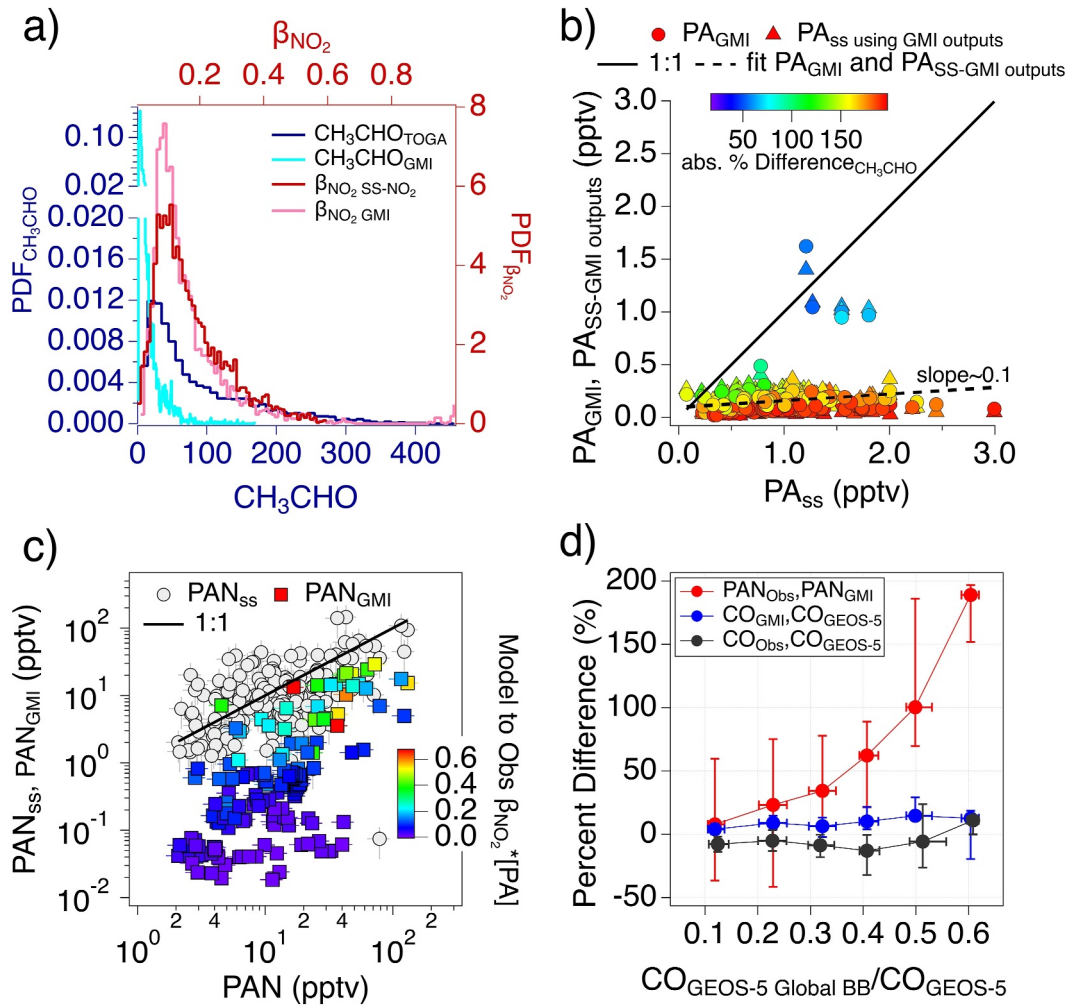

Figure 3. (a) Probability distribution functions of observed and modeled CH_3CHO and β_{NO_2}. (b) Scatter plots of PA concentrations from both the model outputs (PA_{GMI}) and steady state (SS) calculations using modeled precursors ($PA_{SS\text{-}GMI}$) against SS calculations using observations. Data points are color-coded using the absolute percent difference between modeled and observed CH_3CHO. (c) Scatter plots of acetyl peroxynitrate (PAN) from SS calculations (PAN_{SS}) and model simulations (PAN_{GMI}) versus observations. (d) Percent differences between observed and GMI-modeled PAN (red), GMI-modeled and GEOS-5 modeled CO (blue), and observed and GEOS-5 modeled CO (gray), which are illustrated as a function of fractional contribution of CO from global biomass burning ($CO_{GEOS\text{-}5\ Global\ BB}$) to total CO in GEOS-5 in the Southern Hemisphere.

complicated acetaldehyde source attribution (e.g., Millet et al., 2010; Singh et al., 2004; Staudt et al., 2003) were likely minimal given the low detection limit (5 pptv for acetaldehyde) of TOGA enabled by reduced ozone–wall interactions (S. Wang et al., 2019). In contrast, the model underestimated β_{NO_2} more significantly in the lower troposphere, which is consistent with the underestimation in modeled NO_x using both GMI and GEOS-Chem without photolysis of particulate nitrate at altitudes below 6 km, as discussed by Shah et al. (2023). Consistent with this, the 3-D model underestimates the observed PAN levels by 60% and 55% over the NH and SH, respectively.

Figure 3b compares PA concentrations directly from the 3-D model output and those derived from SS calculations using modeled and observed constraints. To be consistent with SS calculations for PAN (Figure 3c), only data with temperatures >290 K were included. On average, PA concentrations from both the model output and SS calculations using modeled PAN precursors were approximately 90% lower than the estimated values based on observations and equations in Supporting Information S1 (SE1-2). Improved agreement between the modeled and observed PA was found when the relative difference between modeled and observed acetaldehyde was reduced.

The remote lower tropospheric conditions observed during ATom facilitate the diagnosis of the model-simulated PAN using SS calculations of PAN. In these conditions, the short τ_{PAN}, persistent acetaldehyde levels and limited perturbation from transport improve validity of the SS calculations (Cleary et al., 2007 and Text S4 in Supporting Information S1). Figure 3c illustrates that observed PAN is in better agreement with the SS estimation than the 3-D model. The agreement between the modeled and observed PAN improves when β_{NO_2} and PA from the 3-D model and observations are consistent. In addition, latitudinal medians of PAN/NO_x further demonstrate observations are more consistent with SS estimations than the 3-D model (Figure S10 in Supporting Information S1). This supports the compatibility between PAN and its precursors and emphasizes the need to better address the model biases in acetaldehyde and β_{NO_2}.

Biomass burning emissions had a significant impact on the remote tropospheric PAN distribution during ATom. Strong linear relationships between PAN and HCN were particularly notable in the SH, where Figure S11 in Supporting Information S1 illustrates this relationship across altitude bins for both the NH and SH observations. To investigate the impact of biomass burning on the observation-model discrepancies in PAN, we focused on the percent difference of PAN between observations and GMI model simulations in the SH due to the relatively simple emission source characteristics dominated by biomass burning. Figure 3d illustrates the percent difference in PAN increased with fractional contribution of CO from global biomass burning in GEOS-5, which is consistent with an increasing percent difference in PAN with observed HCN levels (Figure S11 in Supporting Information S1). The increase in the difference in PAN was found while CO from GEOS-5 agrees with both CO from GMI and observations within 30%. For this reason, we suggest that model simulations of the global PAN distribution will depend on accurate treatment of chemical evolution in biomass burning plumes as well as emissions and transport. Given the dominant role of biomass burning on PAN distributions in the SH, the measurements in this work provide a valuable benchmark for evaluating model simulations.

4. Discussion

This work provides observational evidence for a large and persistent global impact of biomass burning on PAN in the remote troposphere, particularly in the SH. The significant influence is facilitated by the injection of PAN precursors in plumes often transported at higher altitudes, where thermolysis is slower and wind speeds are higher (e.g., Ke et al., 2021). Satellite observations that attributed a significant portion of upper tropospheric and lower stratospheric PAN to pyro-convective transport of biomass burning emissions are in accord with our findings (Moore & Remedios, 2010; Pope et al., 2016; Tereszchuk et al., 2013). Consistent with this, GEOS-CTM implementing a new satellite-based fire plume injection scheme showed the greatly improved agreement between modeled and observed vertical distributions of PAN and CO in North American boreal regions (Zhu et al., 2018).

Efficient PAN production is common in biomass burning plumes (Alvarado et al., 2010; X. Liu et al., 2016; Xu et al., 2021), but simulating this process in CTMs remains challenging due to complex factors such as emissions, plume injection, mixing, and photochemistry (Andreae, 2019; X. Liu et al., 2016; Theys et al., 2020; S. Wang et al., 2021). Our measurements from the FIREX-AQ (Fire Influence on Regional to Global Environments of Air Quality) campaign and earlier field studies show that PAN often constitutes 40%–50% of NO_y a few hours downwind of fires (Alvarado et al., 2010; X. Liu et al., 2016; Xu et al., 2021), likely reflecting these combined effects. While a detailed understanding of PAN chemistry is critical for biomass burning plume evolution, assigning ~40% of biomass burning NO_x to PAN is practical for global PAN simulations by CTMs (e.g., Fischer et al., 2014). However, markedly variable NO_x to PAN conversion rates across fire types (e.g., wildfire and prescribed burning) suggest that implementing conversion rates specific to fire types may be an effective modeling strategy (e.g., X. Liu et al., 2016, 2017). This suggestion aligns with analysis of satellite observations by Jin et al. (2021) which reported both decreasing NO_x lifetime with the magnitude of fire emissions and difficulties in assessing the effects of PAN on the evolution of NO_x using an exponentially modified Gaussian analysis. Consequently, our work suggests that the model treatments of plume transport and conversion of biomass burning NO_x emissions to PAN are an important focus for reliably simulating the global PAN distributions.

5. Conclusion

This work reports global-scale airborne observations of remote tropospheric PAN during the ATom campaign. PAN concentrations over the NH oceans were impacted by a mix of sources such as anthropogenic emissions,

transpacific transport from East Asia, and biomass burning. Biomass burning has a dominant and persistent impact on PAN in the SH. Our diagnostic evaluation of modeled PAN and its precursors based on observations suggests the GMI model, as well as other similar CTMs, should account for the underestimations of acetaldehyde and β_{NO_2} to improve PAN simulations in the lower troposphere. In addition, we suggest that accurate treatment of biomass burning should be a focus for model simulations of PAN in the remote troposphere. The remote tropospheric PAN observations in this work provide a valuable data set for the analyses and evaluation of satellite observations and model simulations.

Data Availability Statement

The data used in this work is available from the ATom campaign archive at https://doi.org/10.3334/ORNLDAAC/1925 (Wofsy et al., 2021). The GMI modelling results for the ATom campaign are available at https://doi.org/10.3334/ORNLDAAC/1897 (Strode et al., 2021).

Acknowledgments
The PAN observations and analysis were supported by NASA Grants NNX15AT90G and 80NSSC23K0826. This material is based upon work supported by the NSF National Center for Atmospheric Research, which is a major facility sponsored by the U.S. National Science Foundation under Cooperative Agreement No. 1852977. The GMI CTM was supported by the NASA Modeling, Analysis and Prediction (MAP) program. The NASA High-End Computing Program (HEC) provided computational resources through the NASA Center for Climate Simulation (NCCS) for the GMI CTM simulation.

References

Allen, H. M., Crounse, J. D., Kim, M. J., Teng, A. P., Ray, E. A., McKain, K., et al. (2022). H_2O_2 and CH_3OOH (MHP) in the remote atmosphere: 1. Global distribution and regional influences. *Journal of Geophysical Research: Atmospheres*, *127*(6), e2021JD035701. https://doi.org/10.1029/2021JD035701

Alvarado, M. J., Logan, J. A., Mao, J., Apel, E., Riemer, D., Blake, D., et al. (2010). Nitrogen oxides and PAN in plumes from boreal fires during ARCTAS-B and their impact on ozone: An integrated analysis of aircraft and satellite observations. *Atmospheric Chemistry and Physics*, *10*(20), 9739–9760. https://doi.org/10.5194/acp-10-9739-2010

Andreae, M. O. (2019). Emission of trace gases and aerosols from biomass burning—An updated assessment. *Atmospheric Chemistry and Physics*, *19*(13), 8523–8546. https://doi.org/10.5194/acp-19-8523-2019

Andreae, M. O., Artaxo, P., Beck, V., Bela, M., Freitas, S., Gerbig, C., et al. (2012). Carbon monoxide and related trace gases and aerosols over the Amazon Basin during the wet and dry seasons. *Atmospheric Chemistry and Physics*, *12*(13), 6041–6065. https://doi.org/10.5194/acp-12-6041-2012

Apel, E. C., Hornbrook, R. S., Hills, A. J., Blake, N. J., Barth, M. C., Weinheimer, A., et al. (2015). Upper tropospheric ozone production from lightning NO_x-impacted convection: Smoke ingestion case study from the DC3 campaign. *Journal of Geophysical Research: Atmospheres*, *102*, 2505–2523. https://doi.org/10.1002/2014JD022121

Blake, N. J., Blake, D. R., Wingenter, O. W., Sive, B. C., McKenzie, L. M., Lopez, J. P., et al. (1999). Influence of southern hemispheric biomass burning on midtropospheric distributions of nonmethane hydrocarbons and selected halocarbons over the remote South Pacific. *Journal of Geophysical Research: Atmopsheres*, *104*(D13), 16213–16232. https://doi.org/10.1029/1999JD900067

Bottenheim, J. W., Sirois, A., Brice, K. A., & Gallant, A. J. (1994). Five years of continuous observations of PAN and ozone at a rural location in eastern Canada. *Journal of Geophysical Research: Atmopsheres*, *99*(D3), 5333–5352. https://doi.org/10.1029/93JD02716

Bourgeois, I., Peischl, J., Neuman, J. A., Brown, S. S., Thompson, C. R., Aikin, K. C., et al. (2021). Large contribution of biomass burning emissions to ozone throughout the global remote troposphere. *Proceedings of the National Academy of Sciences of the USA*, *118*(52), e2109628118. https://doi.org/10.1073/pnas.2109628118

Cleary, P. A., Wooldridge, P. J., Millet, D. B., McKay, M., Goldstein, A. H., & Cohen, R. C. (2007). Observations of total peroxy nitrates and aldehydes: Measurement interpretation and inference of OH radical concentrations. *Atmospheric Chemistry and Physics*, *7*(8), 1947–1960. https://doi.org/10.5194/acp-7-1947-2007

Fischer, E. V., Jacob, D. J., Yantosca, R. M., Sulprizio, M. P., Millet, D. B., Mao, J. F., et al. (2014). Atmospheric peroxyacetyl nitrate (PAN): A global budget and source attribution. *Atmospheric Chemistry and Physics*, *14*(5), 2679–2698. https://doi.org/10.5194/acp-14-2679-2014

Frenzel, A., Kutsuna, S., Takeuchi, K., & Ibusuki, T. (2000). Solubility and reactivity of peroxyacetyl nitrate (PAN) in dilute aqueous salt solutions and in sulphuric acid. *Atmospheric Environment*, *34*(21), 3641–3644. https://doi.org/10.1016/S1352-2310(00)00132-1

Holzinger, R., Warneke, C., Hansel, A., Jordan, A., Lindinger, W., Crutzen, P. J., et al. (1999). Biomass burning as a source of formaldehyde, acetaldehyde, and methanol emissions. *Geophysical Research Letters*, *26*(8), 1161–1164. https://doi.org/10.1029/1999GL900156

Jaffe, D., Anderson, T., Covert, D., Kotchenruther, R., Trost, B., Danielson, J., et al. (1999). Transport of Asian air pollution to North America. *Geophysical Research Letters*, *26*(6), 711–714. https://doi.org/10.1029/1999GL900100

Jin, X., Zhu, Q., & Cohen, R. C. (2021). Direct estimates of biomass burning NO_x emissions and lifetimes using daily observations from TROPOMI. *Atmospheric Chemistry and Physics*, *21*(20), 15569–15587. https://doi.org/10.5194/acp-21-15569-2021

Kasibhatla, P. S., Levy, H., & Moxim, W. J. (1993). Global NO_x, HNO_3, PAN, and NO_y distributions from fossil fuel combustion emissions: A model study. *Journal of Geophysical Research*, *98*(D4), 7165–7180. https://doi.org/10.1029/92jd02845

Ke, Z., Wang, Y., Zou, Y., Song, Y., & Liu, Y. (2021). Global wildfire plume-rise data set and parameterizations for climate model applications. *Journal of Geophysical Research: Atmospheres*, *126*(6), e2020JD033085. https://doi.org/10.1029/2020JD033085

Lee, Y., Huey, L. G., Wang, Y., Qu, H., Zhang, R., Ji, Y., et al. (2021). Photochemistry of volatile organic compounds in the Yellow River Delta, China: Formation of O_3 and peroxyacyl nitrates. *Journal of Geophysical Research: Atmospheres*, *126*(23), e2021JD035296. https://doi.org/10.1029/2021JD035296

Liu, J., Mauzerall, D. L., & Horowitz, L. W. (2005). Analysis of seasonal and interannual variability in transpacific transport. *Journal of Geophysical Research*, *110*(D4), D04302. https://doi.org/10.1029/2004JD005207

Liu, X., Zhang, Y., Huey, L. G., Yokelson, R. J., Selimovic, V., Simpson, I. J., et al. (2017). Airborne measurements of western U. S. wildfire emissions: Comparison with prescribed burning and air quality implications. *Journal of Geophysical Research: Atmospheres*, *122*(11), 6108–6129. https://doi.org/10.1002/2016JD026315

Liu, X., Zhang, Y., Huey, L. G., Yokelson, R. J., Wang, Y., Jimenez, J. L., et al. (2016). Agricultural fires in the southeastern U.S. during SEAC4RS: Emissions of trace gases and particles and evolution of ozone, reactive nitrogen, and organic aerosol. *Journal of Geophysical Research: Atmospheres*, *121*(12), 7383–7414. https://doi.org/10.1002/2016JD025040

Millet, D. B., Guenther, A., Siegel, D. A., Nelson, N. B., Singh, H. B., de Gouw, J. A., et al. (2010). Global atmospheric budget of acetaldehyde: 3-D model analysis and constraints from in-situ and satellite observations. *Atmospheric Chemistry and Physics*, *10*(7), 3405–3425. https://doi.org/10.5194/acp-10-3405-2010

Moore, D. P., & Remedios, J. J. (2010). Seasonality of Peroxyacetyl nitrate (PAN) in the upper troposphere and lower stratosphere using the MIPAS-E instrument. *Atmospheric Chemistry and Physics*, *10*(13), 6117–6128. https://doi.org/10.5194/acp-10-6117-2010

Moxim, W. J., Levy, H., & Kasibhatla, P. S. (1996). Simulated global tropospheric PAN: Its transport and impact on NO_x. *Journal of Geophysical Research*, *101*(D7), 12621–12638. https://doi.org/10.1029/96jd00338

Müller, K. P., & Rudolph, J. (1992). Measurements of peroxyacetylnitrate in the marine boundary layer over the Atlantic. *Journal of Atmospheric Chemistry*, *15*(3–4), 361–367. https://doi.org/10.1007/BF00115405

Nault, B. A., Garland, C., Pusede, S. E., Wooldridge, P. J., Ullmann, K., Hall, S. R., & Cohen, R. C. (2015). Measurements of $CH_3O_2NO_2$ in the upper troposphere. *Atmospheric Measurement Techniques*, *8*(2), 987–997. https://doi.org/10.5194/amt-8-987-2015

Newman, P. A., & Pawson, S. (2021). *ATom: GEOS-5 derived meteorological conditions and tagged tracers along flight tracks*. ORNL Distributed Active Archive Center. https://doi.org/10.3334/ORNLDAAC/1876

Nowak, J. B., Parrish, D. D., Neuman, J. A., Holloway, J. S., Cooper, O. R., Ryerson, T. B., et al. (2004). Gas-phase chemical characteristics of Asian emission plumes observed during ITCT 2K2 over the eastern North Pacific Ocean. *Journal of Geophysical Research*, *119*(D23), DS23S19. https://doi.org/10.1029/2003JD004488

Paton-Walsh, C., Emmerson, K. M., Garland, R. M., Keywood, M., Hoelzemann, J. J., Huneeus, N., et al. (2022). Key challenges for tropospheric chemistry in the Southern Hemisphere. *Elementa Science of the Anthropocene*, *10*, 1. https://doi.org/10.1525/elementa.2021.00050

Penkett, S. A., & Brice, K. A. (1986). The spring maximum in photo-oxidants in the Northern Hemisphere troposphere. *Nature*, *319*(6055), 655–657. https://doi.org/10.1038/319655a0

Pope, R. J., Richards, N. A. D., Chipperfield, M. P., Moore, D. P., Monks, S. A., Arnold, S. R., et al. (2016). Intercomparison and evaluation of satellite peroxyacetyl nitrate observations in the upper troposphere-lower stratosphere. *Atmospheric Chemistry and Physics*, *16*(21), 13541–13559. https://doi.org/10.5194/acp-16-13541-2016

Ray, E. A. (2021). *ATom: Back trajectories and influences of air parcels along flight track 2016–2018*. ORNL Distributed Active Archive Center. https://doi.org/10.3334/ORNLDAAC/1889

Roberts, J. M. (2007). PAN and related compounds. In *Volatile organic compounds in the atmosphere* (pp. 221–268). Blackwell Publishing Ltd. https://doi.org/10.1002/9780470988657.ch6

Roberts, J. M., Flocke, F., Chen, G., de Gouw, J., Holloway, J. S., Hubler, G., et al. (2004). Measurement of peroxycarboxylic nitric anhydrides (PANs) during the ITCT 2K2 aircraft intensive experiment. *Journal of Geophysical Research*, *109*(D23), D23S21. https://doi.org/10.1029/2004JD004960

Roozitalab, B., Emmons, L. K., Hornbrook, R. S., Kinnison, D. E., Fernandez, R. P., Li, Q., et al. (2024). Measurements and modeling of the interhemispheric differences of atmospheric chlorinated very short-lived substances. *Journal of Geophysical Research: Atmospheres*, *129*(2), e2023JD039518. https://doi.org/10.1029/2023JD039518

Rudolph, J., Rudolph-Vierkorn, B., & Meixner, F. X. (1987). Large-Scale distribution of peroxyacetylnitrate results from the STRATOZ III flights. *Journal of Geophysical Research*, *92*(D6), 6653–6661. https://doi.org/10.1029/JD092iD06p06653

Schill, G. P., Froyd, K. D., Brian, H., Kupc, A., Williamson, C., Brock, C. A., et al. (2020). Widespread biomass burning smoke throughout the remote troposphere. *Nature Geoscience*, *13*(6), 422–427. https://doi.org/10.1038/s41561-020-0586-1

Shah, V., Jacob, D. J., Dang, R., Lamsal, L. N., Strode, S. A., Steenrod, S. D., et al. (2023). Nitrogen oxides in the free troposphere: Implications for tropospheric oxidants and the interpretation of satellite NO_2 measurements. *Atmospheric Chemistry and Physics*, *23*(2), 1227–1257. https://doi.org/10.5194/acp-23-1227-2023

Sillman, S., Logan, J. A., & Wofsy, S. C. (1990). The sensitivity of ozone to nitrogen oxides and hydrocarbons in regional ozone episodes. *Journal of Geophysical Research*, *95*(D2), 1837–1851. https://doi.org/10.1029/JD095iD02p01837

Singh, H. B., Brune, W. H., Crawford, J. H., Flocke, F., & Jacob, D. J. (2009). Chemistry and transport of pollution over the Gulf of Mexico and the Pacific: Spring 2006 INTEX-B campaign overview and first results. *Atmospheric Chemistry and Physics*, *9*(7), 2301–2318. https://doi.org/10.5194/acp-9-2301-2009

Singh, H. B., Brune, W. H., Crawford, J. H., Jacob, D. J., & Russell, P. B. (2006). Overview of the summer 2004 Intercontinental chemical Transport experiment–North America (INTEX-A). *Journal of Geophysical Research*, *111*(D24), D24S01. https://doi.org/10.1029/2006JD007905

Singh, H. B., & Hanst, P. L. (1981). Peroxyacetyl Nitrate (PAN) in the unpolluted atmosphere: An important reservoir for nitrogen oxides. *Geophysical Research Letters*, *8*, 941–944. https://doi.org/10.1029/GL008i008p00941

Singh, H. B., Herlth, D., Kolyer, R., Chatfield, R., Viezee, W., Salas, L. J., et al. (1996). Impact of biomass burning emissions on the composition of the South Atlantic troposphere: Reactive nitrogen and ozone. *Journal of Geophysical Research*, *101*(D19), 24203–24219. https://doi.org/10.1029/96JD01018

Singh, H. B., Salas, L. J., Chatfield, R. B., Czech, E., Fried, A., Walega, J., et al. (2004). Analysis of the atmospheric distribution, sources, and sinks of oxygenated volatile organic chemicals based on measurements over the Pacific during TRACE-P. *Journal of Geophysical Research*, *109*(D15), D15S07. https://doi.org/10.1029/2003JD003883

Staudt, A. C., Jacob, D. J., Ravetta, F., Logan, J. A., Bachiochi, D., Krishnamurti, T. N., et al. (2003). Sources and chemistry of nitrogen oxides over the tropical Pacific. *Journal of Geophysical Research*, *108*(D2), 8239. https://doi.org/10.1029/2002JD002139

Stohl, A., Eckhardt, S., Forster, C., James, P., & Spichtinger, N. (2002). On the pathways and timescales of intercontinental air pollution transport. *Journal of Geophysical Research*, *107*, D23–D4684. https://doi.org/10.1029/2001JD001396

Strode, S. A., Liu, J., Lait, L., Commane, R., Daube, B., Wofsy, S., et al. (2018). Forecasting carbon monoxide on a global scale for the ATom-1 aircraft mission: Insights from airborne and satellite observations and modeling. *Atmospheric Chemistry and Physics*, *18*(15), 10955–10971. https://doi.org/10.5194/acp-18-10955-2018

Strode, S. A., Steenrod, S. D., Nicely, J. M., Liu, J., Damon, M. R., & Strahan, S. E. (2021). *ATom: Global Modeling Initiative (GMI) Chemical Transport Model (CTM) Output [Model Output]*. ORNL Distributed Active Archive Center. https://doi.org/10.3334/ORNLDAAC/1897

Talukdar, R. K., Burkholder, J. B., Schmoltner, A.-M., Roberts, J. M., Wilson, R. R., & Ravishankara, A. R. (1995). Investigation of the loss processes for peroxyacetyl nitrate in the atmosphere: UV photolysis and reaction with OH. *Journal of Geophysical Research*, *100*(D7), 14163–14173. https://doi.org/10.1029/95jd00545

Tereszchuk, K. A., Moore, D. P., Harrison, J. J., Boone, C. D., Park, M., Remedios, J. J., et al. (2013). Observations of peroxyacetyl nitrate (PAN) in the upper troposphere by the Atmospheric Chemistry Experiment-Fourier Transform Spectrometer (ACE-FTS). *Atmospheric Chemistry and Physics*, *13*(11), 5601–5613. https://doi.org/10.5194/acp-13-5601-2013

Theys, N., Volkamer, R., Müller, J.-F., Zarzana, K. J., Kille, N., Clarisse, L., et al. (2020). Global nitrous acid emissions and levels of regional oxidants enhanced by wildfires. *Nature Geoscience*, *13*(10), 681–686. https://doi.org/10.1038/s41561-020-0637-7

Thompson, C. R., Wofsy, S. C., Prather, M. J., Newman, P. A., Hanisco, T. F., Ryerson, T. B., et al. (2021). The NASA atmospheric Tomography (ATom) Mission—Imaging the chemistry of the global atmosphere. *Bulletin of the American Meteorological Society*, *103*(3), E761–E790. https://doi.org/10.1175/BAMS-D-20-0315.1

Toma, S., Bertman, S., Groff, C., Xiong, F., Shepson, P. B., Romer, P., et al. (2019). Importance of biogenic volatile organic compounds to acyl peroxy nitrates (APN) production in the southeastern US during SOAS 2013. *Atmospheric Chemistry and Physics*, *19*(3), 1867–1880. https://doi.org/10.5194/acp-19-1867-2019

Travis, K. R., Heald, C. L., Allen, H. M., Apel, E. C., Arnold, S. R., Blake, D. R., et al. (2020). Constraining remote oxidation capacity with ATom observations. *Atmospheric Chemistry and Physics*, *20*(13), 7753–7781. https://doi.org/10.5194/acp-20-7753-2020

Wahner, A., Rohrer, F., Ehhalt, D. H., Atlas, E., & Ridley, B. (1994). Global measurements of photochemically active compounds. *Environmental Science Research: Global Atmospheric-Biospheric Chemistry*, *48*, 205–222. https://doi.org/10.1007/978-1-4615-2524-0_12

Wang, S., Coggon, M. M., Gkatzelis, G. I., Warneke, C., Bourgeois, I., Ryerson, T., et al. (2021). Chemical tomography in a fresh wildland fire plume: A large eddy simulation (LES) study. *Journal of Geophysical Research: Atmospheres*, *126*(18), e2021JD035203. https://doi.org/10.1029/2021JD035203

Wang, S., Hornbrook, R. S., Hills, A., Emmons, L. K., Tilmes, S., Lamarque, J.-F., et al. (2019). Atmospheric acetaldehyde: Importance of air-sea exchange and a missing source in the remote troposphere. *Geophysical Research Letters*, *46*(10), 5601–5613. https://doi.org/10.1029/2019GL082034

Wang, Y., Shim, C., Blake, N., Blake, D., Choi, Y., Ridley, B., et al. (2003). Intercontinental transport of pollution manifested in the variability and seasonal trend of springtime O_3 at northern middle and high latitudes. *Journal of Geophysical Research*, *108*(D21), 4683. https://doi.org/10.1029/2003JD003592

Wofsy, S. C., Afshar, S., Allen, H. M., Apel, E. C., Asher, E. C., Barletta, B., et al. (2021). ATom: Merged atmospheric chemistry, trace gases, and aerosols, version 2 [Dataset]. *ORNL DAAC, Oak Ridge, Tennessee, USA*. https://doi.org/10.3334/ORNLDAAC/1925

Xu, L., Crounse, J. D., Vasquez, K. T., Allen, H., Wennberg, P. O., Bourgeois, I., et al. (2021). Ozone chemistry in western U.S. wildfire plumes. *Science Advances*, *7*(49), eabl3648. https://doi.org/10.1126/sciadv.abl3648

Zhai, S., Jacob, D. J., Franco, B., Clarisse, L., Coheur, P., Shah, V., et al. (2024). Transpacific transport of Asian peroxyacetyl nitrate (PAN) observed from satellite: Implications for ozone. *Environmental Science & Technology*, *58*(22), 9760–9769. https://doi.org/10.1021/acs.est.4c01980

Zhang, L., Jacob, D. J., Boersma, K. F., Jaffe, D. A., Olson, J. R., Bowman, K. W., et al. (2008). Transpacific transport of ozone pollution and the effect of recent Asian emission increases on air quality in North America: An integrated analysis using satellite, aircraft, ozonesonde, and surface observations. *Atmospheric Chemistry and Physics*, *8*(20), 6117–6136. https://doi.org/10.5194/acp-8-6117-2008

Zhu, L., Martin, M. V., Gatti, L. V., Kahn, R., Hecobian, A., & Fischer, E. V. (2018). Development and implementation of a new biomass burning emissions injection height scheme (BBEIH v1.0) for the GEOS-Chem model (v9-01-01). *Geoscientific Model Development*, *11*(10), 4103–4116. https://doi.org/10.5194/gmd-11-4103-2018

References From the Supporting Information

Crounse, J. D., McKinney, K. A., Kwan, A. J., & Wennberg, P. O. (2006). Measurement of gas-phase hydroperoxides by chemical ionization mass spectrometry. *Analytical Chemistry*, *78*(19), 6726–6732. https://doi.org/10.1021/ac0604235

Elkins, J. W., Fahey, D. W., Gilligan, J. M., Dutton, G. S., Baring, T. J., Volk, C. M., et al. (1996). Airborne gas chromatograph for in situ measurements of long-lived species in the upper troposphere and lower stratosphere. *Geophysical Research Letters*, *23*(4), 347–350. https://doi.org/10.1029/96GL00244

Faloona, I. C., Tan, D., Lesher, R. L., Hazen, N. L., Frame, C. L., Simpas, J. B., et al. (2004). A laser-induced fluorescence instrument for detecting tropospheric OH and HO_2: Characteristics and calibration. *Journal of Atmospheric Chemistry*, *47*(2), 139–167. https://doi.org/10.1023/b:joch.0000021036.53185.0e

Hall, S. R., Ullmann, K., Prather, M. J., Flynn, C. M., Murray, L. T., Fiore, A. M., et al. (2018). Cloud impacts on photochemistry: Building a climatology of photolysis rates from the atmospheric tomography mission. *Atmospheric Chemistry and Physics*, *18*(22), 16809–16828. https://doi.org/10.5194/acp-18-16809-2018

Hornbrook, R. S., Hills, A. J., Riemer, D. D., Abdelhamid, A., Flocke, F. M., Hall, S. R., et al. (2016). Arctic springtime observations of volatile organic compounds during the OASIS-2009 campaign. *Journal of Geophysical Research: Atmospheres*, *121*(16), 9789–9813. https://doi.org/10.1002/2015JD024360

Karion, A., Sweeney, C., Wolter, S., Newberger, T., Chen, H., Andrews, A., et al. (2013). Long-term greenhouse gas measurements from aircraft. *Atmospheric Measurement Techniques*, *6*(3), 511–526. https://doi.org/10.5194/amt-6-511-2013

LaFranchi, B. W., Wolfe, G. M., Thornton, J. A., Harrold, S. A., Browne, E. C., Min, K. E., et al. (2009). Closing the peroxy acetyl nitrate budget: Observations of acyl peroxy nitrates (PAN, PPN, and MPAN) during BEARPEX 2007. *Atmospheric Chemistry and Physics*, *9*(19), 7623–7641. https://doi.org/10.5194/acp-9-7623-2009

Lee, Y. R., Ji, Y., Tanner, D. J., & Huey, L. G. (2020). A low-activity ion source for measurement of atmospheric gases by chemical ionization mass spectrometry. *Atmospheric Measurement Techniques*, *13*(5), 2473–2480. https://doi.org/10.5194/amt-13-2473-2020

McKain, K., & Sweeney, C. (2021). *ATom: CO_2, CH_4, and CO measurements from Picarro, 2016–2018*. ORNL DAAC. https://doi.org/10.3334/ORNLDAAC/1732

Payne, V. H., Kulawik, S. S., Fischer, E. V., Brewer, J. F., Huey, L. G., Miyazaki, K., et al. (2022). Satellite measurements of peroxyacetyl nitrate from the Cross-Track Infrared Sounder: Comparison with ATom aircraft measurements. *Atmospheric Measurement Techniques*, *15*(11), 3497–3511. https://doi.org/10.5194/amt-15-3497-2022

Ryerson, T., Williams, E., & Fehsenfeld, F. (2000). An efficient photolysis system for fast-response NO_2 measurements. *Journal of Geophysical Research*, *105*(D21), 26447–26461. https://doi.org/10.1029/2000JD900389

Slusher, D. L., Huey, L. G., & Tanner, D. J. (2004). A thermal dissociation-chemical ionization mass spectrometry (TD-CIMS) technique for the simultaneous measurements of peroxyacyl nitrates and dinitrogen pentoxide. *Journal of Geophysical Research*, *109*, D19315. https://doi.org/10.1029/2004JD004670